Title
RETENTION AND RELEASE OF WATER BY SINTERED URANIUM DIOXIDE

Authors
Olander, D.R.
Sherman, D.
Balooch, M.

Publication Date
1982

LBL-13899
Preprint

Lawrence Berkeley Laboratory
UNIVERSITY OF CALIFORNIA

Materials & Molecular Research Division

Submitted to the Journal of Nuclear Materials

RETENTION AND RELEASE OF WATER BY SINTERED URANIUM DIOXIDE

D.R. Olander, D. Sherman, and M. Balooch

January 1982

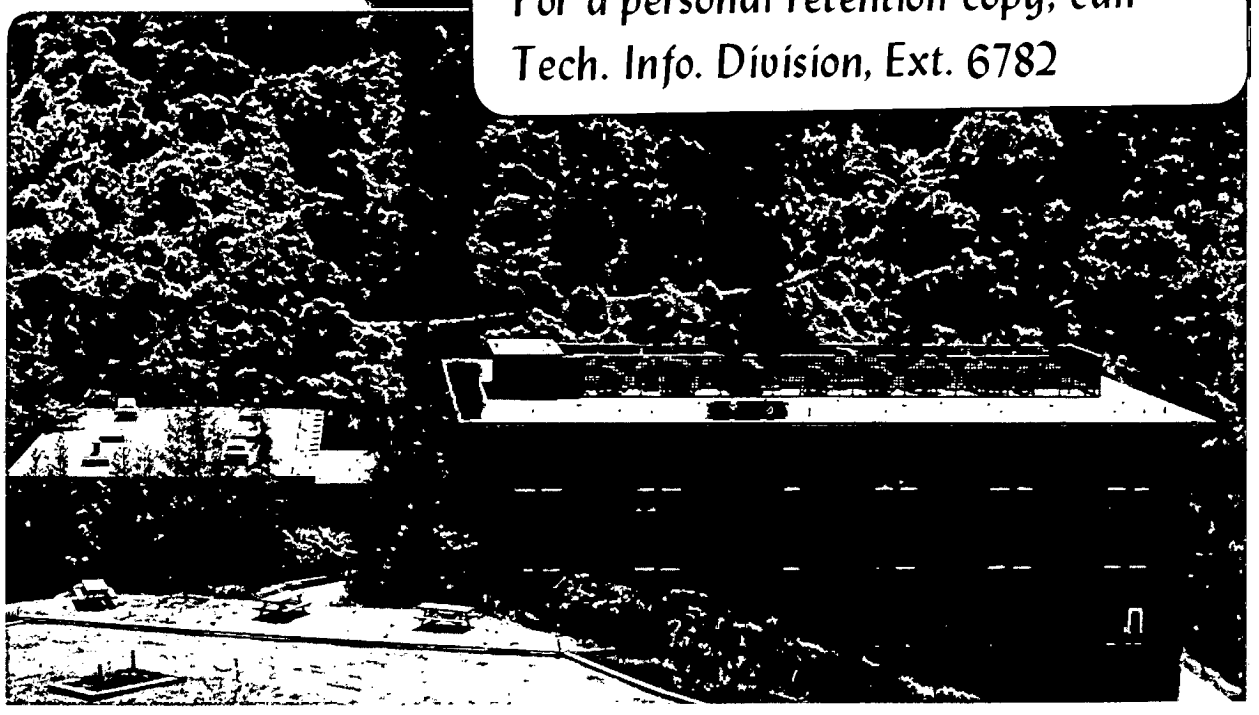

Prepared for the U.S. Department of Energy under Contract W-7405-ENG-48

DISCLAIMER

RETENTION AND RELEASE OF WATER BY SINTERED URANIUM DIOXIDE

D. R. Olander

D. Sherman

and

M. Balooch

Materials and Molecular Research
Division of the Lawrence Berkeley
Laboratory and the
Department of Nuclear Engineering
University of California
Berkeley, California 94720

This work was supported by the Director, Office of Energy Research, Office of Basic Energy Sciences, Materials Sciences Division of the U.S. Department of Energy under contract # W-7405-ENG-48.

ABSTRACT

The release of water and hydrogen upon heating sintered UO_2 pellets was measured by a direct mass spectrometric method of vacuum outgassing. The technique avoids water loss by sample transfer and measures, rather than the cumulative release, the rate of release with a sensitivity level of 1 μg of water (as D_2O) per hour. Exposure of high-density UO_2 pellets to water (liquid D_2O) results in negligible water adsorption. Water in pellets fabricated with especially high open porosity (5%) was driven off by a linear temperature ramp below 200 °C. A drying model for this process was developed and applied to the data. Strongly bound water was introduced into high-density UO_2 by sintering in an atmosphere of D_2O and D_2. Release of the water or hydrogen began at ∿ 500 °C and was complete only at the melting point of UO_2 (2800 °C). The release kinetics are not diffusion-controlled; rather the process is governed by the rates of desorption of bound hydrogen-bearing species from at least three binding sites in the solid characterized by interaction energies between 20 and 50 kcal/mole. The D_2O/D_2 ratio of the desorbed gas was > 1 and did not correspond to thermodynamic equilibrium with stoichiometric urania. Hydrogen and water release kinetics are comparable below ∿ 2000 °C, suggesting a common bound precursor. The total hydrogen (as D_2O or D_2) absorbed in the specimens was between 2 and 4 μg/gUO_2.

I. INTRODUCTION

Sintered uranium dioxide pellets adsorb moisture very rapidly when exposed to the atmosphere(1). When heated, the water vapor desorbs. Unless UO_2 is properly dried before fabrication of fuel elements, released water can cause hydriding of the zircaloy cladding in LWR and CANDU type pins.

Beyer and Hann(2) have reviewed past experience on UO_2 outgassing. Three earlier studies dealing with release of water and other gases from UO_2 are summarized in Table 1. The measurements of gas release were performed by heating the pellets in vacuum and transferring the gas collected to a calibrated volume where gas composition was determined by a mass spectrometer or a gas chromatograph. Although the moisture contents of the storage atmospheres were not reported in any of these studies, pellet exposure to helium appeared to result in smaller water pickup than did storage in air. An unusually large amount of low-temperature release of water was observed by Ferrari(5) for pellets sintered in wet hydrogen. In Ferrari's tests all of the water was released between 50 and 160°C. On the other hand, Spalaris and Magerth(3) found that only ~20% of the total water was released in low temperature tests (<400°C). In the experiments of Denovan, et al(4), less than 40% of the water was removed below 240°C. All three of these experiments are suspect because they could not avoid loss of outgassed water vapor by adsorption on the cool walls of the transfer lines and apparatus surfaces.

Another source of water (or hydrogen) in fuel pellets is the gaseous atmosphere used during sintering. Whether cracked ammonia or wet

hydrogen is utilized for stoichiometry control during sintering, the possibility of retention of hydrogen-bearing gases by the solid during the densification process cannot be discounted. Ferrari(5), for example, studied the high-temperature release of nitrogen from fuel pellets sintered in cracked ammonia.

The main goal of the experiments described above was to determine the quantity of water vapor and other impurity gases released from UO_2 as a function of temperature. The objectives of the present study are to determine the sources of water in UO_2, to measure its instantaneous rate of release in prescribed temperature ramps, and to deduce the mechanisms of the release processes. To avoid problems of measuring small H_2O signals by a mass spectrometer in the presence of a large background of H_2O in the vacuum system, D_2O was used in the study. In addition, direct molecular beam sampling and in situ detection of the released D_2O was employed in place of post-release transfer of the gas to a separate chamber for analysis.

II. EXPERIMENTAL PROCEDURE

A. UO_2 Specimens

The UO_2 samples used in this study were fabricated by the EXXON Nuclear Co. and their characteristics are shown in Table 2. The pellets were approximately 1 cm in diameter and 1 cm in height. Two were used in each outgassing test. The short-time, low-temperature sintering conditions of the type-A pellets resulted in high open and closed porosities (Fig. 1a) and a measurable BET surface area (determined by krypton adsorption). These samples were outgassed at 250°C for 24 hours in vacuum, cooled and immersed immediately in liquid D_2O for 2-4 hours.

Excess D_2O was removed by rolling in a lint-free towel, and the samples were transferred to the crucible and placed in the vacuum system.

The types B and D pellets were prepared under standard commercial fuel sintering conditions. They were approximately 93% of theoretical density but had essentially no open porosity (Fig. 1b). Their surface area was less than the limit of detection of the BET method. The type-B pellets were loaded with D_2O using the method described above for the type-A pellets. The type-D pellets were not exposed to D_2O.

Exposure to the atmosphere or immersion in liquid water are not the only means of introducing hydrogen into UO_2 pellets. In all sintering operations, hydrogen is present in the sintering gas, either as a hydrogen-nitrogen mixture or, as in the present case, as wet hydrogen. In order to ascertain whether this exposure to hydrogen-bearing gases during the sintering step results in retention of some of the hydrogen, the type-C pellets were fabricated. The sintering conditions for these specimens were the same as those of the Types B and D compacts except that the sintering gas was D_2 saturated with D_2O instead of the usual H_2O/H_2 mixture. These pellets were introduced into the release apparatus without additional treatment.

B. Release Apparatus

The apparatus shown in Fig. 2 consists of a CVD tungsten crucible placed in a vacuum resistance furnace. Temperatures are measured by a thermocouple touching the outside of the crucible or, for high temperatures, by an optical pyrometer sighted on the bottom of the crucible. The lip on the tungsten crucible is sealed to a molybdenum flange-capillary assembly by a platinum gasket. All gases leave the crucible

via a small-bore capillary tube which is aimed directly at the ionizer of a quadrupole mass spectrometer several centimeters distant. In this way, the gases are delivered in free-molecule flow to the mass spectrometer detector. The molybdenum flange-capillary assembly is heated independently to at least 100°C to prevent adsorption of condensible D_2O on cold metal surfaces. The pumpout time of the crucible-capillary combination was calculated to be less than 0.5 sec. Thus the system samples all of the gases released from the UO_2 specimen with a very small time constant. The signal derived from the mass spectrometer via the lock-in amplifier is proportional to the instantaneous rate of release of the species of interest from the sample in the crucible.

The rate at which D_2O leaves the crucible via the sampling tube is measured using a modulated molecular beam technique. Before the molecular beam formed by effusion from the sampling tube reaches the ionizer of the mass spectrometer, it is periodically interrupted by a three-bladed chopper rotating at a modulation frequency of 50 Hz. The output signal of the mass spectrometer (tuned to mass 20 for D_2O or to mass 4 for D_2) is an a.c. signal from the direct (modulated) gas flow from the sampling tube superimposed on a d.c. background signal due to D_2O or D_2 which has not yet been pumped out of the vacuum system. The output signal from the mass spectrometer is fed into a lock-in amplifier, which discriminates against the d.c. component of the signal and responds only to that part of the signal which has a frequency equal to that of the 50 Hz reference signal from the beam chopper. The modulated beam technique permits measurement of signals which are only 0.1% of the d.c. background signal.

In order to quantitatively convert the mass spectrometer output signal to a release rate of D_2O from the UO_2 pellets, calibration of the system is required. For this purpose, the crucible is fitted with an input line coming from a chamber outside of the vacuum system which contains a calibration gas (see Fig. 2). By allowing the calibration gas to flow into the crucible at a known rate and recording the mass spectrometer signal due to this flow, absolute calibration of the mass spectrometer can be accomplished. The end of the calibration line runs close to and parallel with the crucible exit capillary, so that both lines have the same geometric view of the mass spectrometer ionizer. Keeping the lines separate up to the vacuum avoids backflow of released gases up the calibration line. Calibration was accomplished with neon gas which is easier to handle than D_2O vapor. The latter strongly adsorbs on all cool metal surfaces and reliable determination of flow rate by measurement of pressure decrease in the known calibration tank volume is difficult to achieve. However, in a separate experiment, the mass spectrometer signal for D_2O was found to be 3 times that of neon for the same flow rate, and this factor was used to convert the neon calibration signal to an equivalent D_2O sensitivity of the mass spectrometer. The system was calibrated before and after each run, and occasionally during an experiment.

In an earlier publication using a similar apparatus (6), substantial quantities of D_2O, initially adsorbed on the UO_2 at low temperature, were reported to have been released at temperatures well above 1000°C. It was later discovered that the same type of signals were observed when the mass spectrometer was tuned to mass 9, where no signal is expected.

Data reported in Ref. 6 are thus false, being solely due to electronic pickup from the furnace current by the mass spectrometer. To avoid this problem, the mass spectrometer was encased in the aluminum sheath shown in Fig. 2 A blank was run to verify that the detection system no longer responded to spurious electronic noise which varied with the current flowing through the heating element of the furnace. The noise level of the entire system was found to be equivalent to a D_2O release rate of 0.5 - 1 μg/hr.

III. DESORPTION OF PHYSICALLY ADSORBED WATER (Pellet types A and B)

A. Results

Water physically adsorbed on the available surfaces of the type-A and type-B pellets was desorbed by a linear temperature ramp which followed an 18-hr ambient temperature outgassing period in the release apparatus.

Two type-B specimens were tested with temperature ramps of 250°C/hr and 900°C/hr, respectively. Some D_2O emission during the initial stages of the 18-hr room temperature outgassing periods was observed, undoubtedly arising from removal of water on the geometric surfaces of the pellets. Thereafter, neither of the samples tested showed any D_2O release up to the maximum temperature tested (1750°C). The D_2O signals recorded by the mass spectrometer were at the noise level of the system (<1 μg/hr) at all times. Since the type-B pellets had neither open porosity nor measurable internal surface area (Table 2), the absence of physically adsorbed water is understandable.

The type-A pellets were tested in a similar manner, with a temperature ramp of 185°C/hr initiated after 18 hours of room temperature vacuum outgassing. The release rate during the isothermal period

decreased rapidly at first but leveled off at a value between 90 and 100 μg/hr during the few hours prior to initiation of the temperature increase (at t = 0). During the temperature transient (Fig. 3) the release rate rose rapidly to a peak of nearly 500 μg/hr at 3/4 hr. It then decayed smoothly and approached another constant value of ∿20 μg/hr between 1-1/2 and 2 hours. At this time, the temperature ramp was increased to 295°C/hr, which produced another, smaller peak in the D_2O release rate. This secondary peak decayed slowly and the system noise level (<1 μg/hr) was reached at a temperature of ∿1000°C.

The course of the water release process is shown in a cumulative fashion in Table 3. After immersion in D_2O, all of the open porosity of the pellets is filled with liquid (this is the basis for determining open porosity). By the time that the first release rate measurement was made following placement of the sodden specimen in the vacuum system, only 4.4% of the initial water remained. By the start of the temperature ramp, 99.7% of the D_2O had been removed by the process of transferring the specimen to the vacuum system, pumping down, and vacuum outgassing at room temperature for 18 hr.

The last column of Table 3 shows the fractional coverage of the internal surfaces of the pellets by D_2O, assuming this to be uniform. Knowledge of the BET surface area (S) and the formula (7):

$$S = \frac{q_m A N_{av} x 10^{-26}}{M_w} \qquad (1)$$

permits the monolayer coverage by $D_2O(q_m)$ to be computed. In Eq(1), M_w is the molecular weight of D_2O and N_{av} is Avogadro's number. The quantity A is the projected area of a water molecule in a monolayer, which is taken to be 13 $\AA^2$ (7). For S = 0.14 m^2/g (Table 2), q_m is found to be 36 μg D_2O/g and the fractional coverages in the last column of Table 3 are obtained by dividing this figure into those in the second column.

Table 3 shows that the vast majority of the water is removed before the first measurement, and most of what remains escapes to the vacuum during the initial constant temperature outgassing period. On a volume basis, the temperature transient releases only the last dregs of D_2O in the specimen. However, on a surface coverage basis, the 0.3% of water remaining at the start of the temperature ramp provides a surface coverage of 0.5 if uniformly spread over all accessible internal surfaces of the porous specimen. It is, however, more likely that the water at this stage is concentrated towards the interior of the pellets, with the internal surfaces closest to the vacuum having been largely depleted of adsorbed water. The internal surfaces near the center of the pellet would then have fractional coverages greater than one.

B. Drying Model

The literature on drying of porous solids contains numerous examples of isothermal drying curves such as the one shown in Fig. 4. In this schematic, the ordinate is equivalent to the release rate and the abcissa is the percent of the pore volume filled by liquid water (shown in the third column of Table 3 for the present experiment). Three stages of drying are depicted: a constant-rate period due to evaporation of water

from the outer surface of the solid with the pores full, and two falling-rate periods, usually associated with vapor transport first in connected porosity (two-pore evaporation) then in isolated pores (one-pore evaporation). This schematic and the data in Fig. 3 for t<0 both indicate that a nonzero drying rate is sustained as the water content of the body approaches zero. Conventional analyses designed to model bulk drying (8) do not predict such a nonzero intercept; rather, the drying rate should smoothly approach zero as the last dregs of water are removed. Consequently, there must be another mechanism involved, one which is capable of sustaining a nearly constant drying rate until practically all of the water is exhausted from the body. This feature of the drying process is evident by the following data: at t =-5 hrs, the specimen contains ∿50 μg D_2O/g which decreases to ∿18 μg/g at t = 0. Yet during this period, the release rate diminishes from ∿103 μg/hr to ∿92 μg/hr. The problem therefore is to find a release model which permits a factor of nearly 3 decrease in the quantity of adsorbed water at the same time that the release rate decreases by only ∿11%.

This remarkable aspect of the experimental drying curve serves to eliminate a mechanism in which the rate of release is controlled by desorption of water from the internal surfaces of the porous body. In the absence of transport limitations in the pores, the release rate in such a model is obtained from the equation:

$$\frac{dq}{dt} = - B \qquad (2)$$

where q is the quantity of adsorbed water per gram of UO_2 and B is the desorption rate constant. For B = constant, the release rate (which is proportional to dq/dt) is proportional to the quantity adsorbed,

which is not in agreement with the isothermal data. It is known that the rate constant B can depend upon the amount of water remaining on the surface. In order to explain a slowly varying release rate for large decreases in the quantity adsorbed, B would have to increase as q decreases. In a study of water desorption from TiO_2, however, Micale and Zettlemoyer (9) found just the opposite behavior, namely, that B decreases as q decreases. Hence, it is clear that the simple desorption process as expressed by Eq. (2) is not adequate for describing the data.

The type of water release rate observed at the end of the constant temperature period resembles boiloff from a teakettle with the spout closed by a lid with a small hole. If the water in the teakettle is maintained at a constant temperature just above the boiling point corresponding to ambient pressure, the boiloff rate is independent of the amount of water remaining in the kettle. Evaporation ceases instantaneously just when the last drop of liquid is evaporated.

The removal of the last dregs of water during the final portion of the isothermal outgassing period and in the temperature transient is assumed to occur by evaporation from pores in the body in which the principal resistance to transport is a constriction which acts like the hole in the lid of a teakettle. These "teakettle" pores need not communicate directly with the outside surface of the pellet. In fact, they are very likely connected to the main pore system which controls bulk drying of the initial 99.7% of the water in the specimen.

The "teakettle" or "inkbottle" pore shown in Fig. 5 has been invoked in the literature (10) to explain certain features of the adsorption of condensible gases by porous solids. Water vapor is released from the pore at a rate controlled by the conductance k of the constriction. If

there are N such pores per gram of solid, the D_2O release rate R is given by:

$$R = NMkp \tag{3}$$

where M is the mass of solid and p is the pressure inside the pores. Since the part of the pore downstream of the constriction offers no resistance to mass transport, the pressure here is zero. The part of the pore upstream of the constriction contains q_1 μg of D_2O which is related to the water pressure p via an adsorption isotherm. If the mass of water in the vapor phase is neglected, the water mass balance on a pore is:

$$\frac{dq_1}{dt} = -kp \tag{4}$$

In order to utilize the common adsorption isotherms, it is convenient to express the quantity of adsorbed water in terms of the fractional coverage Θ, defined by:

$$\Theta = \frac{q_1}{q_{1m}} \tag{5}$$

where q_{1m} is the number of micrograms of water adsorbed on the pore surface at monolayer coverage. The water pressure inside the pore is expressed in terms of the vapor pressure of bulk water at temperature T by the dimensionless pressure:

$$P = \frac{p}{p_s f(T)} \tag{6}$$

where p_s is the vapor pressure of water at $T_o = 293$ K and

$$f(T) = \exp\left[-\frac{L}{1.98T_o}\left(\frac{T_o}{T} - 1\right)\right] \tag{7}$$

is the fractional increase in the vapor pressure when the temperature is increased from T_o to T. L is the latent heat of water in calories per mole.

In terms of the dimensionless pressure P and the coverage Θ, Eq (4) can be written:

$$\frac{d\Theta}{dt} = - \frac{Pf(T)}{\tau} \tag{8}$$

where

$$\tau = \frac{q_{1m}}{kp_s} \tag{9}$$

is a characteristic time.

In order to integrate Eq. (8) over the final portion of the constant temperature period and through the thermal transient, we need to know the temperature of the solid as a function of time and the isotherm which relates Θ to P and T.

The temperature of the crucible was measured by the thermocouple contacting the wall. However, because the experiments were conducted in vacuum, the sole mode of heat transfer between the crucible wall and the sample was by radiation, and therefore the UO_2 temperature lagged the measured temperature. The temperature measured during the transient is shown as the dashed curve in Fig. 3 and a simple lumped-capacity heat transfer calculation gives the sample temperature history shown as the dotted curve. During most of the transient, the sample temperature lags the wall temperature by $\sim$ 20 min, or, at a given time, the former is $\sim$60 °C lower than the latter.

The BET isotherm is used to describe the adsorption equilibrium because it has been used in the past to determine specific surface areas

of solids by water adsorption (10) and also because it applies to multi-layer adsorption. The BET isotherm is (10) :

$$\Theta = \frac{1}{1 - P} - \frac{1}{1 + (c-1)P} \qquad (10)$$

where c is a measure of the relative binding of water molecules to the bare substrate and to bulk liquid water:

$$c = \exp\left[\frac{E_1 - L}{1.98T}\right] \qquad (11)$$

In Eq (11) E_1 is the binding energy of the molecules to the bare surface, which is generally larger than the binding energy in the bulk liquid represented by the latent heat L. However, for strongly hydrogen-bonded liquids such as water, E_1 may be less than L, in which case parameter c in the BET theory is less than unity. This produces adsorption isotherms called type-III, which are convex to the pressure axis (10). Only this type of isotherm is capable of fitting the release rate data during the constant temperature part of Fig. 3 because it allows a small change in P and Θ. Since the release rate is proportional to P and Θ decreases with time, the type-III isotherm is capable of rationalizing the release rate behavior during the final stage of room temperature drying before the temperature transient. Of course, it should also be able to fit the data during the temperature ramp as well.

If R_o and P_o denote the release rate and dimensionless pressure, respectively, at t = 0, Eq (3) and (6) yield:

$$R_o = NMkp_s P_o \tag{12}$$

The release rate at any time is

$$R = NMkp_s Pf(T) \tag{13}$$

Dividing these two equations gives:

$$R = R_o\left(\frac{P}{P_o}\right)f(T) \tag{14}$$

The quantity adsorbed at t = 0, q_o, is given by:

$$q_o = Nq_{1m}\Theta_o \tag{15}$$

where Θ_o is the fractional coverage of the pores at t = 0.

Dividing Eqs (12) and (15) gives the characteristic time of Eq (9) as:

$$\tau = \frac{q_o M}{R_o}\,\frac{P_o}{\Theta_o} \tag{16}$$

Fitting the experimental data to this release model has been accomplished by the following procedure:

For a given isotherm [e.g., Eq(10) along with specification of E_1 in Eq (11)], the conditions at t = 0 can be determined as follows. The dimensionless pressure at t = 0, P_o is guessed, Θ_o corresponding to this guess of P_o is computed from Eq (10) and τ determined by Eq (16) (q_o and R_o are experimental values). Then Eq (8) is integrated backwards

in time from t = 0 to t = -1.75 hrs using Eq (10) at T = 293 K to relate Θ to P. This integration produces the value of P at -1.75 hrs and application of Eq (14) with f(T) = 1 gives the ratio of the release rates at these two times:

$$\frac{R(t = -1.75)}{R_o} = \frac{P(t = -1.75)}{P_o}$$

When this calculated release rate ratio is equal to the value obtained from the data, the correct value of P_o has been chosen, thereby fixing conditions prior to the temperature ramp. The parameters characterizing the adsorption isotherm are determined by matching the theoretical curve for the thermal transient to the release rate data in Fig. 3 for $t > 0$. The theoretical release rate is obtained by integrating Eq (8), using the adsorption isotherm to relate Θ to P, and calculating R from Eq (14). The maximum release rate, the time at which it occurs, the width of the release rate peak and the cumulative release during the transient are used in the fitting procedure. When used in conjunction with the conventional BET isotherm, Eq (10), only one adjustable parameter is available, namely, E_1 in Eq (11). However, no value of E_1 provided satisfactory agreement of theory and experiment; the theoretical release rates rose rapidly to a maximum approximately twice as large as that observed experimentally and then fell abruptly to zero.

A number of modifications to the simple model were investigated in order to obtain better agreement. What was needed was a means of slowing down the release rate during the temperature ramp without changing the predictions at $t < 0$. The model changes investigated were of three general types, involving either introduction of additional capacity into

the system, modification of the pore geometry or the mass transport relation, or alteration of the adsorption isotherm. Of these variants, only the last produced a reasonably good fit to the experimental data.

Although there has been no experimental study of water adsorption on UO_2, Parfitt (11) has reviewed the extensive literature on water interaction with TiO_2. These studies reveal two states of water adsorbed on this oxide, one characteristic of low coverages and which is strongly bound to the bare surface and a weakly bound second state which is adsorbed on top of the first layer. The strongly bound state appears to exist up to monolayer coverage and exhibits a distinctly different type of adsorption isotherm than the loosely bound overlayer, which reflects normal physical adsorption. It is evident that a simple BET isotherm cannot adequately represent the adsorption properties of such an interaction.

We attempted to apply the notion of two distinct binding states with the change from one to the other at a critical coverage to the UO_2/H_2O system. To implement this adsorption model, we assume normal physical (i.e., BET) adsorption for coverages greater than a critical value Θ_{crit} and allow for a different Θ - P relationship at lower coverages. The critical coverage should be approximately equal to unity, but its exact value depends on the nature of the packing of the water molecules on the surface at the transition point. Figure 6 shows the types of isotherms which were investigated. For $\Theta > \Theta_{crit}$, all variants were assumed to follow curve a, which is a Type-III BET isotherm. If the dashed continuation of curve a is used, the simple model described at the beginning of this section is recovered. Curves b, c, and d represent possible adsorption

isotherms for the strongly bound state present at $\Theta < \Theta_{crit}$. The linear relationship (type b) is the type found for water on TiO_2 (11). Type c is also linear in the region $\Theta < \Theta_{crit}$ but exhibits a discontinuity at Θ_{crit}. This type of isotherm (a → c) is the surface analog of the oxygen potential of UO_{2+x}, which shows a discontinuity at perfect stoichiometry. The type d isotherm at low coverages was taken to be parabolic so that it approximately represents the Freundlich isotherm which fits adsorption of CO_2 on UO_2 reasonably well (12). The low-coverage portion of the isotherm is:

$$P = P_{crit} \left(\frac{\Theta}{\Theta_{crit}}\right)^2 \qquad (17)$$

At $\Theta = \Theta_{crit}$, this branch joins the BET branch, so that P_{crit} and Θ_{crit} are related by Eq (10). For coverages greater than the critical value, Eq (10) rather than Eq (17) applies.

The basic features of these mixed isotherms are intended to reflect the release rate data of Fig. 3. The large coverages characteristic of the outgassing period prior to the temperature transient allow the BET part of the isotherm to produce a slowly-varying release rate (or dimensionless pressure) despite substantial loss of water (large variation in Θ). At some time during the transient, which depends upon the value of the starting coverage Θ_o and the critical coverage Θ_{crit}, the adsorption equilibrium switches to the b, c, or d branches. By reducing the equilibrium pressure of water in the pores below what would have prevailed had the dashed curve a been followed, this switch reduces the release rate. This has the effect of lowering the peak outgassing rate and at the same time extending the release to higher temperatures (i.e., longer times) than predicted by the simple model.

The hybrid isotherms of Fig. 6 were tested within the framework of the rest of the simple model - only the isotherm was changed. The a → b and a → d combinations contain two adjustable parameters, namely, E_1 for describing the BET portion and Θ_{crit} to fix the critical coverage. The a → c combination isotherm contains three parameters.

Extensive data fitting trials showed that the type a → b isotherm did not provide a sufficiently large reduction in equilibrium pressure at low coverages to dramatically improve the agreement of theory to data. The discontinuous a → c isotherm reduces to the a → b type if the discontinuity at Θ_{crit} vanishes, but as the discontinuity becomes larger, the theory predicts two desorption peaks. However, it was not able to reproduce the data on Fig. 3 no matter what magnitude of discontinuity was chosen.

Only the case a → d with the parabolic isotherm at low coverage provided a satisfactory fit to the data. This model is plotted as the solid line on Fig. 3. The parameters deduced from the data fitting procedure were:

$$E_1 = 9.6 \text{ kcal/mole and } \Theta_{crit} = 1.5$$

The coverage of the pore surfaces at t = 0 corresponding to these parameters was found to be $\Theta_o = 2.3$ and the characteristic time of Eq (9) τ, was 1.1 hours.

Based on an area of 13 Å^2 per water molecule, which is typical of the values found for application of the BET isotherm to a variety of water-solid systems (7), the critical coverage separating the submonolayer and multilayer adsorption regimes corresponds to 13/1.5 = 8.7 Å^2 per water molecule. This surface density is approximately equal to the area per oxygen ion on the low Miller index planes of UO_2, and so is not unreasonable.

The value of E_1 determined by the data fitting process is ~ 0.8 kcal/mole less than the latent heat of water, and corresponds to the binding of water molecules to the strongly adsorbed monolayer which exhibits the isotherm given by Eq (17).

The specific surface area of the solid attributable to the teakettle pores of the model can be roughly estimated. The figure of 13 $Å^2$ per water molecule corresponds to 0.026 μg D_2O per cm^2 of surface at monolayer coverage. If there are N pores/g each with a monolayer capacity of q_{1m} μg D_2O, the specific surface area associated with the teakettle pores is $Nq_{1m}/0.026$. In the basic release model, Nq_{1m} is equal to q_o/Θ_o (Eq (15)). where q_o = 18.3 μg D_2O and Θ_o = 2.3, as determined in the data fitting process. Using these figures, the specific surface area of the teakettle pores is ~0.03 m^2/g, which is ~1/5 of the total specific surface area given in Table 1 for the Type-A specimens used in the experiment.

The release rate predicted by the model using the a → d isotherm of Fig. 6 is shown as the solid curve in Fig. 3. The agreement with the data is excellent, except at the very end of the transient. There is apparently a small amount of more strongly bound water than accounted for in the model, which is responsible for the small secondary release peak due to the second temperature ramp and to the persistence of small D_2O release signals up to ~1000 °C.

IV RELEASE OF STRONGLY BOUND WATER

A. Results

Besides exposure at room temperature to atmospheric moisture, UO_2 pellets can pick up water or hydrogen during the sintering process. In order to study the quantity absorbed by this means and its release kinetics, specimens designated as type C in Table 2 were tested. These experiments

were performed with 14.2 g samples. In two runs (Nos. 4 and 5) the mass spectrometer was tuned to mass 20 to detect D_2O. In Run No. 7 deuterium (mass 4) was monitored. Run No. 6 was a blank using virgin pellets (type D in Table 2). The purpose of this last test was to determine the system background, which was found to produce a signal equivalent to a D_2O release rate of 1 ± 0.1 μg/hr, essentially independent of temperature.

In Run No. 4, the temperature was raised quickly to 910°C, held there for 1½ hr, and then raised to a new anneal temperature. This procedure was repeated to a maximum temperature of 2720 °C. Because of the high temperatures involved in this series of tests, the transient response of the furnace was rapid; the new temperature level was attained in ∿ 1 minute following the change in heater power. This time is short compared to duration of the anneals, so that the temperature history of the specimen can be accurately represented by a staircase function. The D_2O release rate in Run No. 4 is shown in Fig. 7. The duration and temperatures of the individual anneals are shown in the lower part of the figure. Following each step change in temperature, the D_2O release rate increased abruptly and then decayed rapidly with time. The sharp leading edges of the release curves characteristic of the anneals at temperatures below 2000 °C gradually became blunted at higher temperatures and disappeared above 2500 °C. This behavior is attributed to a change in the release mechanism. At high temperatures, the last vestiges of D_2O in the specimens are released only when the solid is vaporized. Because of the axial temperature gradient in the crucibles, which were cooler at the top than at the bottom, the UO_2 was found after the experiments as a solid block about 4 cm above the bottom of the crucible where the pellets had been originally placed.

This movement of the specimens is due to vapor transport in UO_2, and insured complete release of D_2 or D_2O. A total of 3.2 μg D_2O/g UO_2 was removed from the specimen in Run No. 4.

Figure 8 shows the D_2O release rates from Run No. 5, which was intended to replicate Run No. 4. The only procedural difference was an initial anneal at 550 °C. As in Run No. 4, this test showed sharp leading edges followed by rapid decay of the D_2O release rate during low temperature anneals. The release rate peaks at higher temperatures were not as rounded as they were in run No. 4. The total quantity of water contained in the specimen used in Run No. 5 was 1.2 μg D_2O/g UO_2. A significant feature of the D_2O release rate response to the temperature changes in Runs 4 and 5 is the lack of dependence of the decay rate on temperature.

The D_2 release from the type-C pellets during step changes in temperature is shown in Fig. 9. The ordinate of this plot has been multiplied by a factor of five to give the equivalent D_2O release rate (i.e. the D_2O release rate which would have been observed had all of the D_2 been oxidized to D_2O). Because the D_2 release rates were very small at low temperature, the first constant-temperature anneal in Run No. 7 was 1620 °C. The rate of decay of the D_2 signal in this and the subsequent anneal was approximately equal to that of D_2O in the same temperature intervals of Runs 4 and 5; for anneals at about 1620 °C, both the D_2O and the D_2 release rates decreased by a factor of 5 - 10 in one hour. The cumulative D_2O-equivalent release in Run No. 7 was 0.5 μg/g UO_2.

B. Model of High Temperature Release

Experiments similar to those reported here were conducted by Ferrari using nitrogen impurity in UO_2(5). For the same type of temperature history, increases in release rate coincident with temperature changes were observed,

followed by a decay to low rates. Ferrari interpreted this behavior as a consequence of a diffusion-controlled process in the solid, although no quantitative development of this thesis was presented. However, simple arguments demonstrate that the data of Figs. 7 and 8 for water and Ferrari's results for nitrogen are incompatible with a diffusional process.

When the diffusion equation appropriate to this type of problem is solved by the separation of variables method, an infinite series of exponentially-decaying terms is obtained (13). After a sufficiently long time, the rapidly decaying terms disappear and only the fundamental mode remains. In this limit, the release rate R is given by:

$$R \propto \exp\left(-\frac{\pi^2 Dt}{a^2}\right) \tag{18}$$

where D is the diffusion coefficient of the solute in the solid and $\underline{a}$ is the effective radius of the spherical body from which release of solute occurs. The tail ends of the release rates in each of the first five anneals of Runs 4 and 5 are compatible with Eq (18) and give values of D/a^2 between 0.1 and 0.2 hr^{-1}, independent of temperature.

A second consequence of applying a diffusional model to interpret the present experiments is that the jump in release rate which occurs with each step increase in temperature provides a direct measurement of the activation energy of diffusion. The release rate just prior to a step temperature change (denoted by subscript -) can be expressed by:

$$R_- \propto -D_-(\partial C/\partial r)_{r=a} \tag{19}$$

where D_- is the diffusion coefficient at the temperature T_- of the anneal prior to the step temperature change and $(\partial C/\partial r)_{r=a}$ is the concentration gradient of water at the surface at the moment that the temperature is changed. The new temperature is attained in a time short compared with the duration of the anneal, so that the release rate following the temperature jump (designated by the subscript +) is given by

$$R_+ \propto - D_+(\partial C/\partial r)_{r=a} \tag{20}$$

where D_+ is the diffusion coefficient at the temperature T_+ of the next anneal. Because the temperature change is rapid (order of minutes) compared to the characteristic time of diffusion (order of hours) the concentration profile in the solid does not change significantly during the temperature change. Therefore the ratio of the rates of release after and before a step change in temperature is:

$$\frac{R_+}{R_-} = \frac{D_+}{D_-} = \exp\left[-\frac{E_D}{k}\left(\frac{1}{T_+} - \frac{1}{T_-}\right)\right] \tag{21}$$

where k is Boltzmann's constant. Treatment of the data in Figs. 7 and 8 as suggested by Eq (21) produces a remarkably precise activation energy for diffusion of E_D = 30 kcal/mole. This behavior is incompatible with the observation that the first five anneals of both runs also obey Eq (18) with a constant value of D, which requires E_D = 0. Thus the release rate data cannot be attributed to a diffusional process, even one which includes solute trapping and resolution, as has been applied to release of fission gases from UO_2 (14).

One possible mechanism which on its face is consistent with the shapes of the experimental release rate curves involves specimen microcracking during temperature jumps. If the transport process leading to water release is Knudsen diffusion through a network of cracks, the diffusion coefficient would not be as temperature-sensitive as true solid state diffusion. The as-received samples had neither measurable open porosity nor detectable BET surface area (Table 2). It is possible, however, that the thermal stresses which accompany the sudden changes in temperature to which the samples were subjected could have created a crack network which permitted escape of water from the pellet interior. To test this possibility, a pellet was raised from a low temperature to $\sim$ 1000 °C at the same rate that was employed in the release tests and then slowly cooled. The pellet was removed from the furnace and its open porosity and BET surface area remeasured. It showed neither. Because of this lack of confirmation of the supposed microcracking due to temperature ramping, the explanation of the water release rates by this type of microstructural modification was rejected.

With diffusional and morphological models found wanting, desorption-limited mechanisms were investigated. A simple desorption-limited release rate is one which is governed by a relation of the type given by Eq (2). The integrated form of this equation exhibits the decaying exponential character displayed by the experimental data. However, the simple desorption rate equation suffers from the same inability to reconcile the jump in release rate with a step temperature change (which requires the desorption rate constant to be activated) and the constancy of the exponential decay at each temperature level (which demands a zero activation energy for desorption).

The simple desorption model is "simple" because it assumes that water is bound to UO_2 on sites all of the same binding energy. However, in a substance as structurally complex as polycrystalline UO_2, characterization of the interaction by a single energy is undoubtedly an oversimplification. Instead, we consider that water in UO_2 is located in binding sites with a distribution of interaction energies. Each site is characterized by a desorption rate constant B hr^{-1} which is assumed to depend on temperature according to:

$$B = A\, e^{-E/kT} \tag{22}$$

where A is the pre-exponential factor and E is the binding energy of water to the site in the solid. The sites are characterized by the parameters A and E, both of which are undoubtedly distributed over a wide range. In order not to introduce into the model more parameters than can be deduced from the data, the pre-exponential factor is assumed to be unique. Thus, the sites are identified only by their binding energies, and the UO_2-water interaction is defined completely by the function $n_s(E)$. The physical meaning of the distribution $n_s(E)dE$ is the mass of water (in μg) per gram of UO_2 bound with energies between E and E + dE to sites in the solid when all available sites are filled with water.

For analysis of the release rates during the sequence of the constant temperature anneals which constitutes each experiment, the binding energy distribution must be converted to the corresponding distribution of desorption rate constants. The latter is designated as $N_s(B)dB$, and means the mass of water (in μg) per gram of UO_2 completely filling sites in the solid on which bound water at temperature T has desorption rate constants between B and B + dB. The two distributions are related by:

$$N_s(B)dB = n_s(E)dE$$

The variables B and E are related by Eq (22), so that at constant temperature the above equation becomes:

$$N_s(B) = n_s\Big(kT\ln(A/B)\Big)\,(kT/B) \qquad (23)$$

The calculation procedure begins by selecting upper and lower bounds E_{min} and E_{max} of the binding energy distribution. These energies roughly depend on the temperatures at which desorption is observed. Then the function $n_s(E)$ is guessed in the range $E_{min} \leq E \leq E_{max}$ (actually the interval is divided into a fixed number of smaller intervals so that a histogram rather than a smooth curve is guessed). The distribution is normalized by requiring that it contain all of the water per gram of UO_2 (denoted by Q_{tot}) which is ultimately released in the first five anneals:

$$Q_{tot} = \int_{E_{min}}^{E_{max}} n_s(E)\,dE \qquad (24)$$

This condition assumes that all binding sites are filled with water at the beginning of the experiment.

Next a value of the pre-exponential factor A is determined by requiring that the theoretical release rate at the beginning of the first anneal of the experiment match the measured value, which provides the restriction:

$$R(\text{start of first anneal}) = \int_{B_{min}}^{B_{max}} B\,N_s(B)\,dB \qquad (25)$$

where the distribution $N_s(B)$ is obtained from the specified binding energy distribution by use of Eq (23). B_{min} and B_{max} are obtained from E_{max} and E_{min}, respectively, by application of Eq(22), in which T is the temperature of the anneal in question.

The adsorption sites are filled with water only at the start of the experiment. For other anneals, whose starting time is denoted by t_o, the fractional filling of the binding sites initially is denoted by $\Theta_o(B)$. This is obtained from the site filling fraction at the end of the preceding anneal, except for the first anneal for which $\Theta_o(B) = 1$. At time t during an anneal, the fractional filling of the adsorption sites is $\Theta(B)$ which is determined by the desorption rate law:

$$\frac{d\Theta}{dt} = - B\Theta$$

or

$$\Theta(t,B) = \Theta_o(B)e^{-Bt} \tag{26}$$

The theoretical release rate during the anneal is:

$$R(t) = \int_{B_{min}}^{B_{max}} B\Theta(t,B)\ N_s(B)\ dB$$

By use of the preceding equations, a guess of the binding site distribution $n_s(E)$ is converted to a prediction of the release rates R(t) for all five anneals in an experiment. The theory is forced to agree with experiment at the beginning of the first anneal and with the total water released during the five anneals considered in the analysis. However, the jump in the release rate which occurs at each change of temperature and the decay of the release rate during each anneal is predicted by the theory for the distribution $n_s(E)$ selected. The results of fitting the release rate data from Runs 4 and 5 are shown as the dashed lines in Figs. 7 and 8. The distribution functions which produced these curves are shown in Figs. 10 and 11 for Runs 4 and 5, respectively. For the specimen used in Run No. 4, three binding sites appear from the analysis at approximate

energies of 25, 40 and 53 kcal/mole. For the specimen of UO_2 used in Run No. 5, four peaks at 18, 26, 37, and 48 kcal/mole, appear. Except for the low energy peak, which is missing in Run No. 4, there is fair agreement in the three high energy peaks between the two runs. The low energy peak may have been missed in Run No. 4 because of the relatively high temperature selected for the first anneal. As can be seen from Figs. 7 and 8, the binding site distributions of Figs. 10 and 11 provide excellent agreement with the experimental release rates.

A procedure identical to that utilized for analyzing the water release curves was applied to the D_2 release data shown in Fig. 9. The binding site distribution shown in Fig. 12 was deduced from the anneals at 1620°C and 1870°C and produced the dashed curves shown in Fig. 9. Because D_2 release was not observed below 1600°C, only binding sites at $\sim$36 and $\sim$46 kcal/mole were found.

C. The Source of the Strongly-Bound Water and Hydrogen

It is clear that the D_2O and D_2 released from the type C pellets at temperatures up to the melting point of UO_2 originated in the sintering gas used during pellet fabrication. However, the gases were not released in the same ratio as they existed in the sintering gas, which was $\sim$ 90% D_2 and 10% D_2O. On the other hand, the cumulative releases from Figs. 7 - 9 demonstrate that the hydrogen-bearing gases released are between 75 and 90% D_2O. Either D_2O was preferentially retained by the fuel during sintering or trapped D_2 was oxidized during release.

The temperatures of the first two anneals in which D_2 was monitored (Fig. 9) were approximately equal to the temperatures of the last two anneals in which D_2O release was measured. In their common temperature range, the decay constants of the D_2 and D_2O signals were comparable, which suggests that, below $\sim$ 2000 °C at least, desorption of a common species is the rate-limiting process in both cases. Interconversion of D_2 to D_2O occurs in the fuel or on its surface during the rapid transport step which follows desorption. The D_2O/D_2 ratio of the gases released in anneals above 1000 °C is between 1 and 3, which is compatible with stoichiometric UO_2 only at temperatures in excess of $\sim$ 2200 °C. Thus it appears that complete equilibrium of the released hydrogen-bearing gases with the oxygen potential of the fuel does not occur. The apparent absence of D_2 below $\sim$ 1600 °C may have been due to difficulties in detection of small release rates of this species, which has a much lower mass spectrometric sensitivity than does D_2O. On the other hand, the absence of D_2 at low temperatures may reflect a kinetic restriction on the decomposition of D_2O released from the solid.

The similarity in the shapes of the D_2 and D_2O release curves vanishes at temperatures greater than $\sim$ 2000 °C. At higher temperatures, the D_2O release rates following a temperature change do not appear to decay more rapidly at higher temperature than at lower temperature. The D_2 release rates in Fig. 9, on the other hand, exhibit a distinct increase in rapidity of decay at high temperatures, approaching an order of magnitude drop in less than 10 minutes. This behavior indicates that different processes control the desorption of D_2 and D_2O at high temperatures.

Both the D_2O release rate in the anneal at 2450 °C of Run No. 5 and the D_2 release rate during the 2590 °C anneal showed a burst in the middle

of the isothermal heating period. These pulses may have been due to opening of previously closed pores in the specimens.

Although the release experiments suggest that a hydrogen-bearing species which ultimately appears as water or molecular hydrogen is bound in UO_2 at several binding sites, no information is obtainable concerning the nature of these sites, nor the chemical form of the bound species. The source of hydrogen and water may have been sintering gas trapped in the closed porosity at the sintering temperature. For a solid with 7% closed porosity formed at 1750 °C in 1 atm of 10% D_2O in D_2, the total equivalent D_2O is 0.9 μg/g UO_2. This value is a factor of three smaller than the quantity of D_2O observed. Consequently, hydrogen-bearing species must be bound to other defects in the polycrystalline solid, of which grain boundaries or dislocations are obvious candidates. If the 3.2 μg D_2O/g UO_2 released in Run No. 4 were uniformly distributed over all grain boundaries in the polycrystalline sample and the grain size is taken to be 10 μm, the area per D_2O molecule (or its precursor) would be $\sim$ 30 Å^2. This value is about twice the projected area of a water molecule, and implies $\sim$ 50% coverage of the grain boundaries if these are indeed the repositories of bound hydrogen in UO_2.

V CONCLUSIONS

Two distinct sources of hydrogen are present in oxide nuclear fuel pellets. The first, which has received sporadic attention in the past, arises from room-temperature adsorption of water on internal open porosity of the fabricated pellets. This source of hydrogen is released (as water) at temperatures in the neighborhood of 100°C. The second source

of hydrogen, which has not heretofore been reported, is due to occlusion of hydrogenous gases employed in pellet sintering. This is released only at temperatures in excess of ∿1000°C in the form of water, accompanied by smaller amounts of elemental hydrogen. Fuel vaporization is required to remove all of this type of retained hydrogen from UO_2.

Models were developed to rationalize both of these release processes. For the low-temperature water, release is believed to occur from internal open pores which communicate with the exterior by a constriction through which water vapor must pass (teakettle pores). The relation between the driving pressure for the release flux and the water content of the solid was found to be best represented by a BET isotherm, modified to account for more strongly bound water at low coverage.

Hydrogen or water retained in fuel during fabrication is released by a process which is not diffusion-controlled. However, a model based on desorption kinetics from binding sites in the solid with a distribution of energies proved satisfactory.

ACKNOWLEDGEMENT

The preparation of the special UO_2 pellets for this work by L. Gerald of EXXON Nuclear Co. is gratefully acknowledged. This work was supported by the Director, Office of Energy Research, Office of Basic Energy Sciences, Materials Sciences Division of the U.S. Department of Energy under contract # W-7405-ENG-48.

REFERENCES

1. R. A. Proebstle, J. H. Davies, T. C. Rowland, D. R. Rutkin, and J. S. Armijo, "The Mechanism of Zircaloy-Clad Fuel Rod Failure by Internal Hydriding", NEDO-20684 (1975).

2. C. E. Beyer and C. R. Hahn, "Release of Indigenous Gases from LWR Fuel and the Reaction Kinetics with Zircaloy Cladding", BNWL-1956 (1977).

3. C. N. Spalaris and F. H. Magerth, "Residual and Fission Gas Release from Uranium Dioxide", GEAP-4314 (1963).

4. A. S. Denovan, R. W. Ashley and T. H. Longhurst, "Internal Sources of Hydrogen in Unirradiated UO_2 Fuel Elements", AECL-4063 (1971).

5. H. M. Ferrari, Nucl. Sci. and Engin., 17, 503 (1963).

6. A. K. Srivastava and D. R. Olander, Trans. Amer. Nucl. Soc., 28, 216 (1978).

7. S. J. Gregg, "The Surface Chemistry of Solids", 2nd Ed., Chapman and Hall (1965).

8. R. B. Keey, "Drying Principles and Practice", Chap. 7, Pergamon (1972).

9. F. J. Micale and A. C. Zettlemoyer, J. Colloid and Interface Sci., 24, 464 (1967).

10. S. J. Gregg and K. S. W. King, "Adsorption, Surface Area and Porosity", Academic Press (1967).

11. G. D. Parfitt, in "Progress in Surface and Membrane Science", D. A. Cadenhead and J. F. Danielli, Eds., p. 181, Academic Press (1976).

12. C. A. Colmenares and K. Terada, J. Nucl. Mater., 58, 336 (1975).

13. H. S. Carslaw and J. C. Jaeger, "Conduction of Heat in Solids", 2nd Ed., Oxford (1959).

14. D. R. Olander, "Fundamental Aspects of Nuclear Reactor Fuel Elements", Sec. 15.6, Nat'l. Info. Tech. Serv. (1976).

Table 1. Previous Studies of Water Release from Uranium Dioxide Pellets

Source	Pellet density, % TD	Storage atmosphere	Release Conditions Temp., °C	Time, min	Water released µg/g UO_2
Spalaris & Magerth (3)	94	helium	1500-1700	7	0.4
Denovan et al (4)	97.5	air	800-1100	-	0.7
Ferrari (5)	-	air	50-160	110	23[a] 0.6[b]

a. pellets sintered in wet hydrogen

b. pellets sintered in cracked ammonia

Table 2. UO_2 Specimens Used in Outgassing Experiments

Type	Sintering Conditions	Porosity, % open	Porosity, % closed	BET surface area, m^2/g	D_2O loading method
A	1450°C, in H_2O/H_2, 2 hrs	5.1	15	0.14	immersion in boiling D_2O liquid
B	1750°C, in H_2O/H_2, 6 hrs	<0.1	7.	<0.01	immersion in boiling D_2O liquid
C	1750°C, in D_2O/D_2, 6 hrs	<0.1	7.	<0.01	D_2 sintering gas saturated with D_2O at 30 - 40°C
D	1750°C, in H_2O/H_2, 6 hrs	<0.1	7.	<0.01	none

Table 3. Water Remaining in the Type-A sample at various times during outgassing

Time, hr	Water remaining in sample, μg D_2O/g	Percent of water in sodden pellet	Fraction of monolayer coverage
after immersion	5600	100	-
start of outgassing (t-18)	246	4.4	6.8
start of heating (t=0)	18.3	0.3	0.5
increase temperature ramp (t=2)	0.5	0.01	0.014

FIGURE CAPTIONS

1. Photomicrographs of UO_2 pellets. (a) type-A pellet; (b) type-B pellet.
2. Apparatus for measuring release of water from UO_2.
3. D_2O release rate from two type-A pellets (16.2 g UO_2); o = data. (a) during initial 18-hr outgassing at 20 °C; (b) during temperature transient.
4. Typical isothermal drying curve of a porous body (after Ref. 8).
5. A teakettle pore.
6. Hybrid water adsorption isotherms used in modeling of the release rate from the teakettle pores. (a) BET isotherm (type-III); (b) linear low coverage continuation of BET isotherm; (c) linear but discontinuous low coverage continuation of BET isotherm; (d) parabolic low coverage continuation of BET isotherm.
7. D_2O release rates during a series of constant temperature anneals during Run No. 4. The background (0.07 μg/hr-g UO_2) has been removed from the raw data.
8. Release rates of D_2O during Run No. 5. Background removed.
9. Deuterium release from UO_2 pellets measured in Run No. 7.
10. Binding site energy distribution deduced from the release rate data for Run No. 4 (Fig. 7).
11. Binding site energy distribution deduced from the release rate data for Run No. 5 (Fig. 8).
12. Binding site energy distribution deduced from the release rate data for Run No. 7 (Fig. 9).

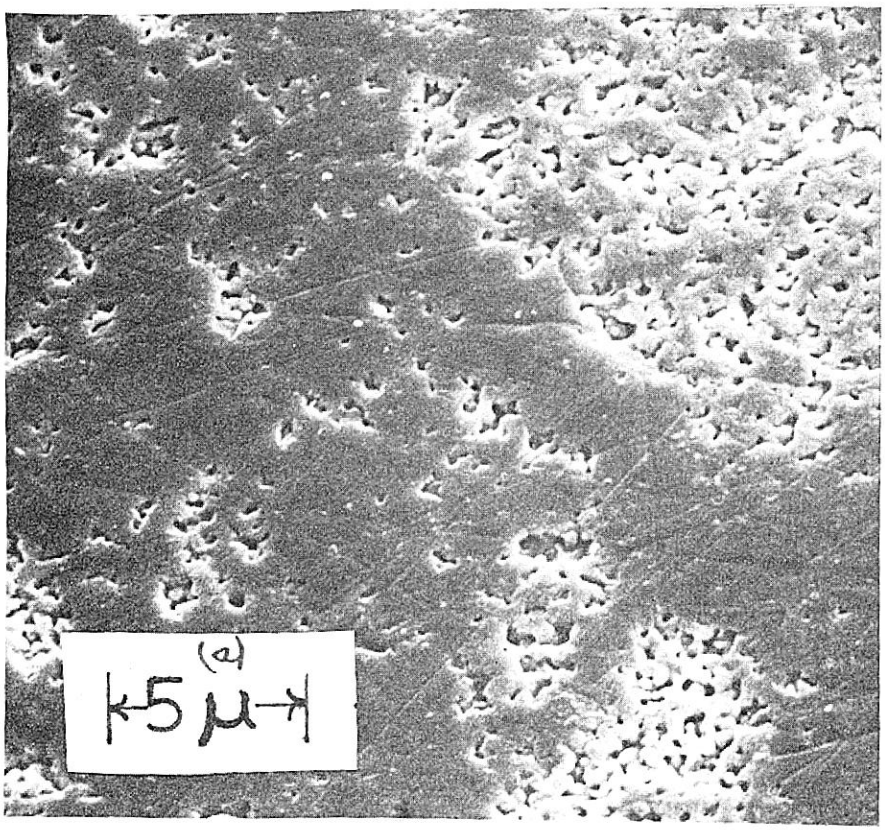

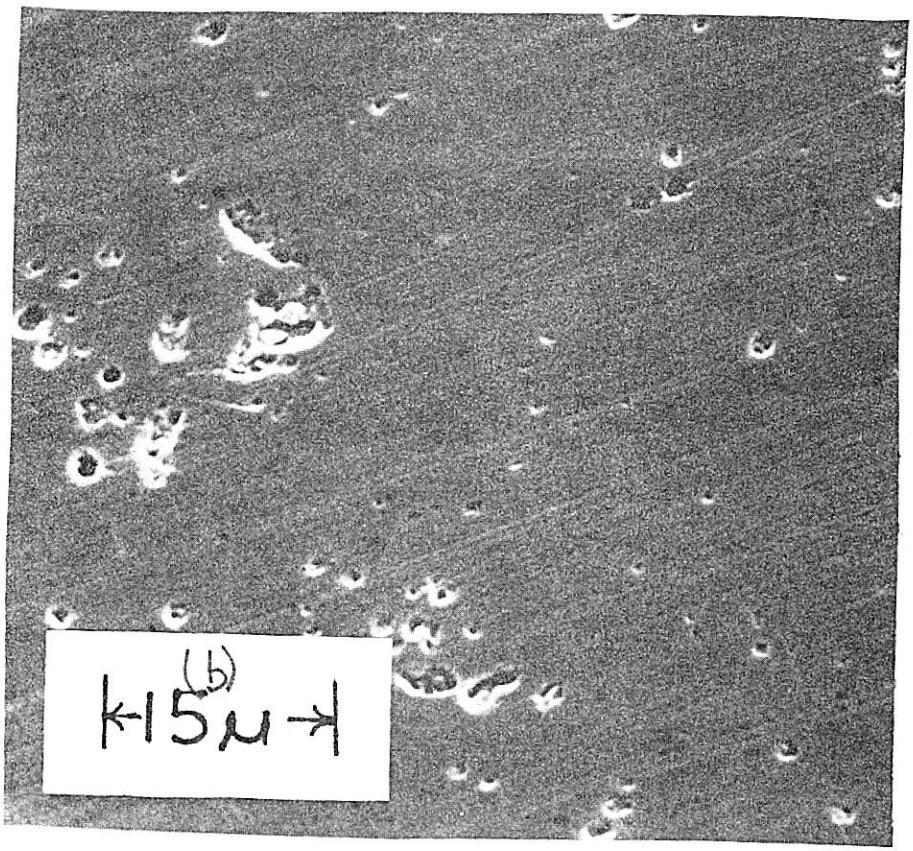

Fig. 1 XBB 804-4147A

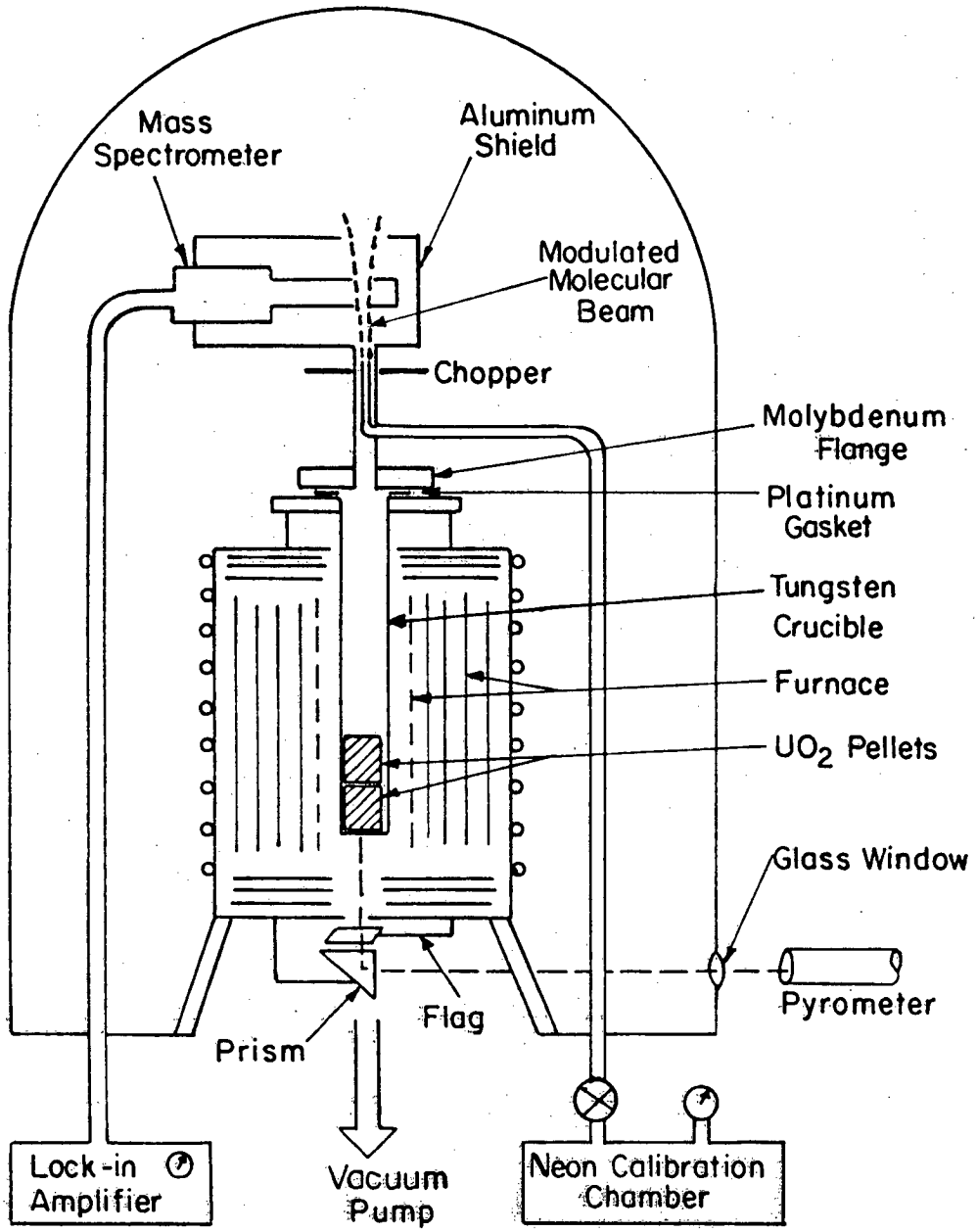
Mass Spectrometer
Aluminum Shield
Modulated Molecular Beam
Chopper
Molybdenum Flange
Platinum Gasket
Tungsten Crucible
Furnace
UO_2 Pellets
Glass Window
Pyrometer
Flag
Prism
Lock-in Amplifier
Vacuum Pump
Neon Calibration Chamber
XBL 791-5625

Fig. 2

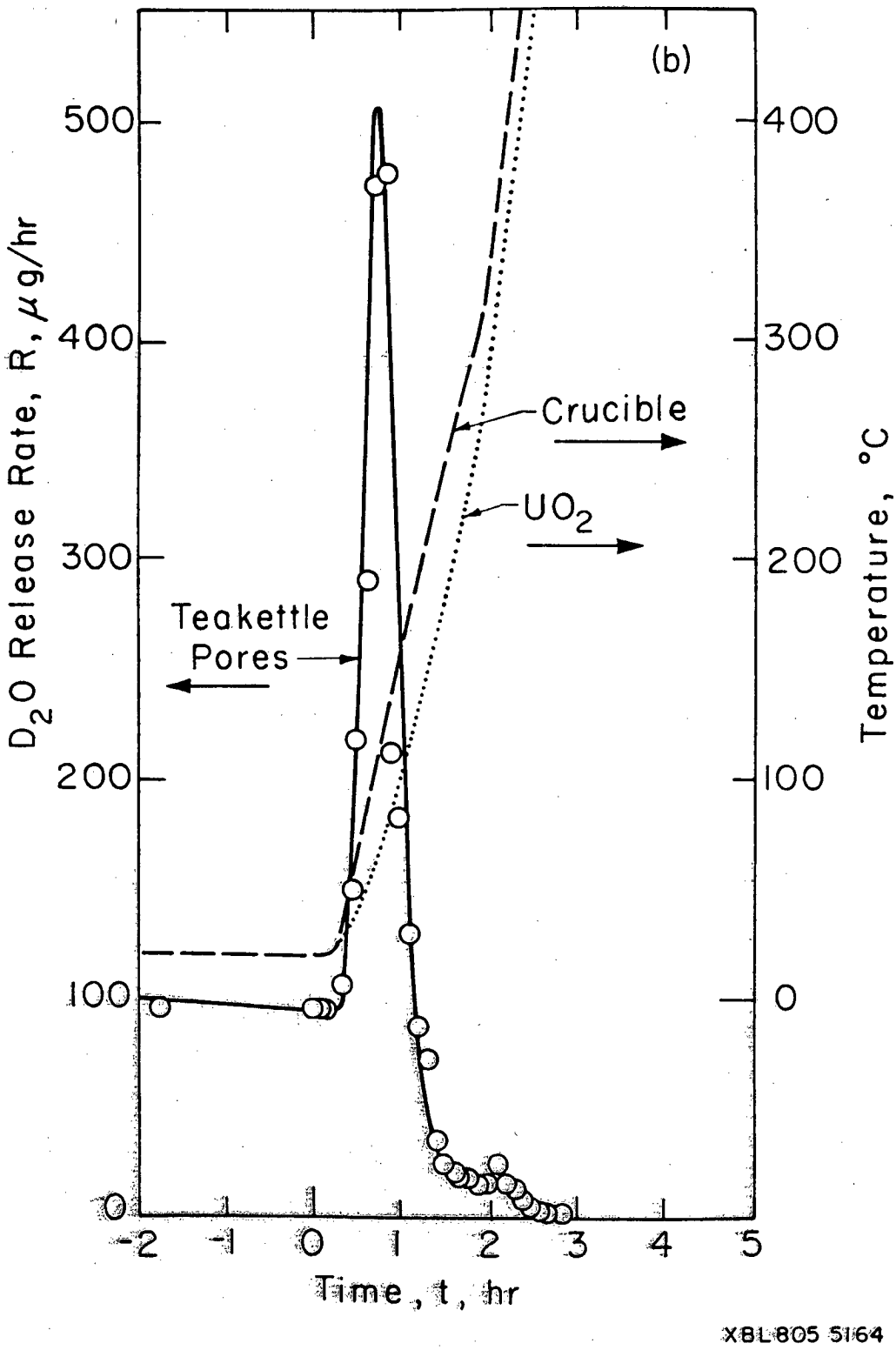
(b)
500
400
300
200
100
0
400
300
200
100
0
D_2O Release Rate, R, μg/hr
Temperature, °C
Crucible
UO_2
Teakettle
Pores
-2
-1
0
1
2
3
4
5
Time, t, hr
XBL805 5164

Fig. 3

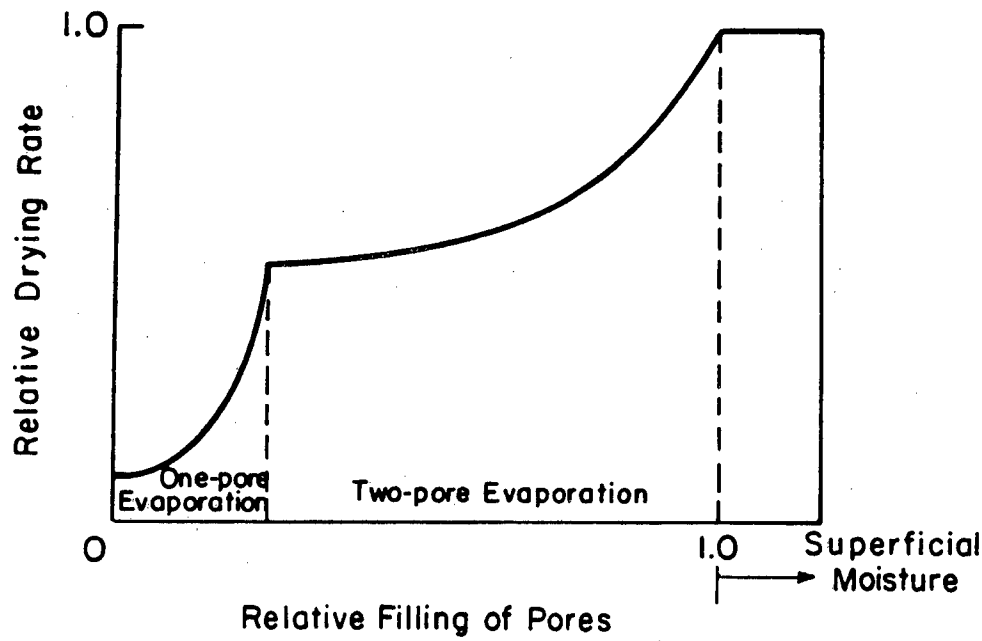
1.0
Relative Drying Rate
One-pore Evaporation
Two-pore Evaporation
0
1.0
Superficial Moisture
Relative Filling of Pores
XBL 805-5165

Fig. 4

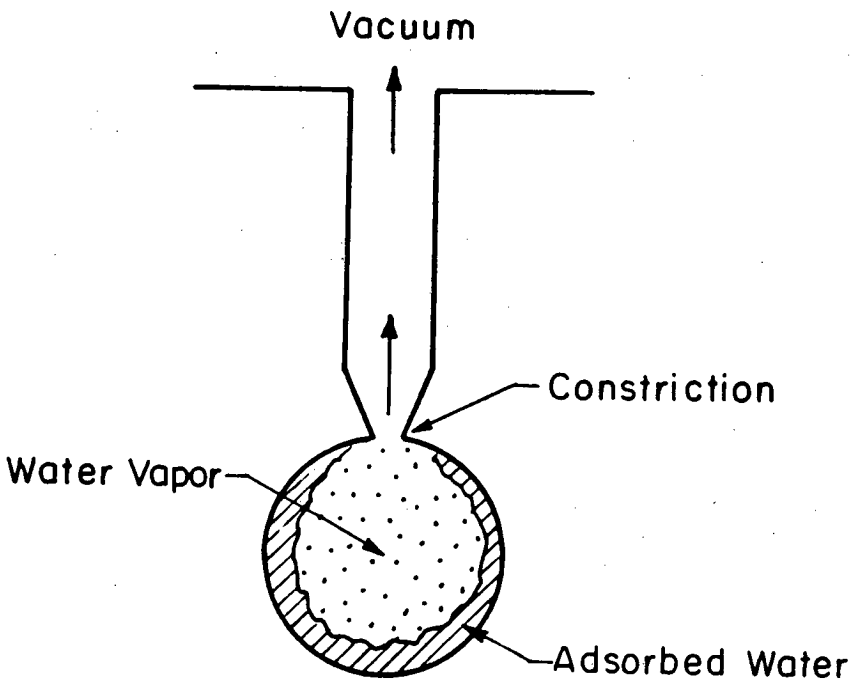
Vacuum
Constriction
Water Vapor
Adsorbed Water
XBL 805-5166

Fig. 5

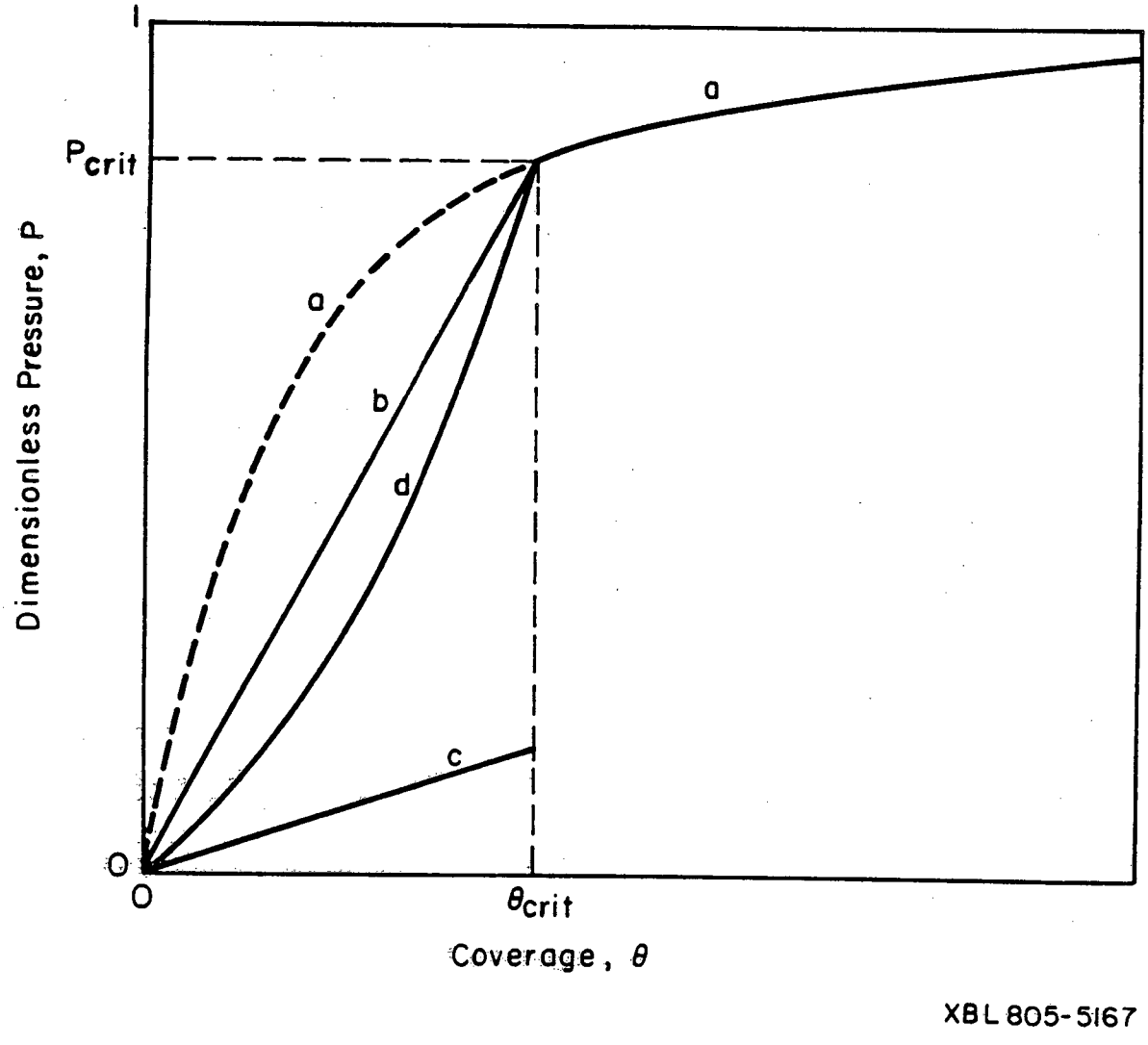
1
P_{crit}
a
a
b
d
c
O
O
θ_{crit}
Dimensionless Pressure, P
Coverage, θ
XBL 805-5167

Fig. 6

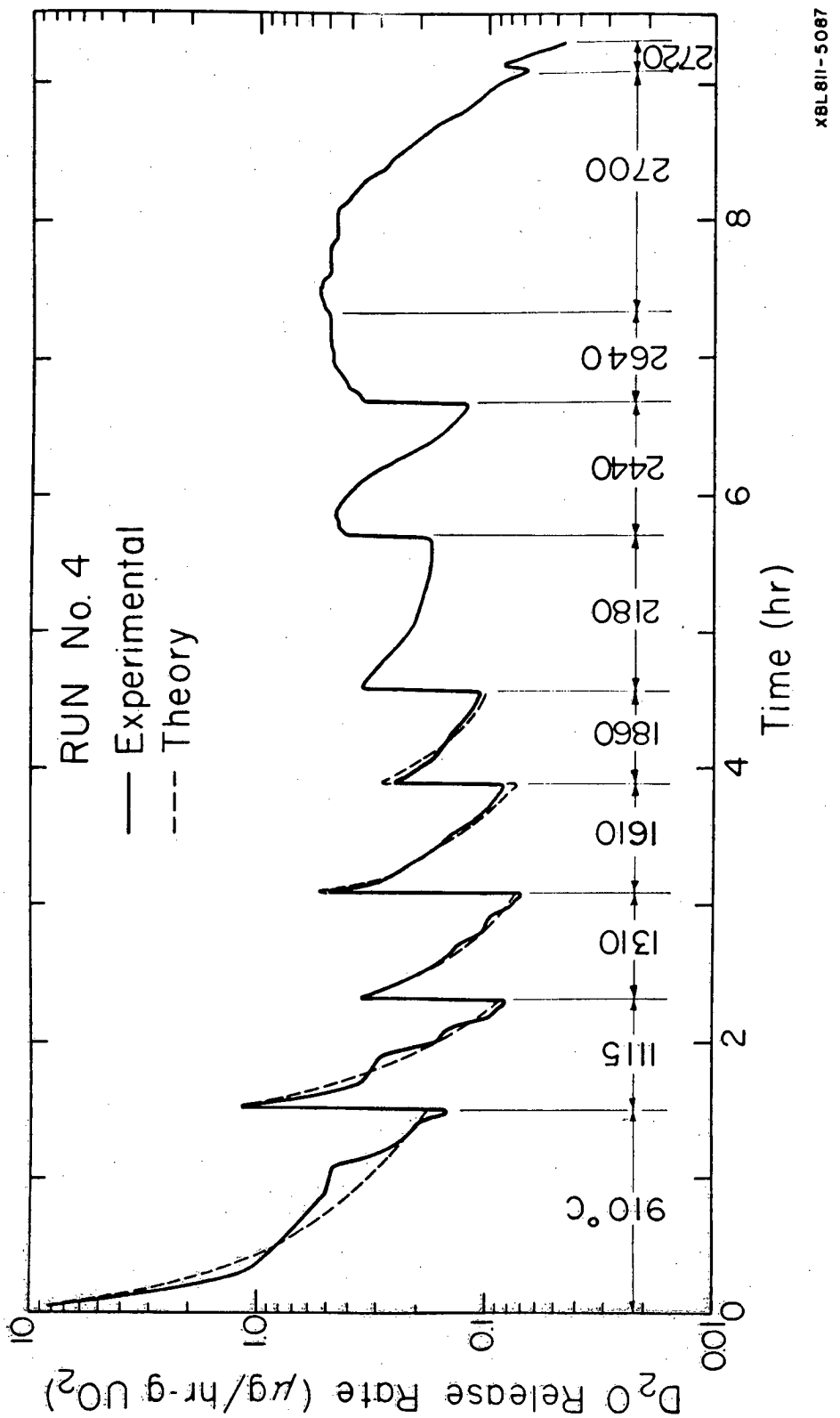
RUN No. 4
Experimental
Theory
910°C
1115
1310
1610
1860
2180
2440
2640
2700
2720
Time (hr)
D_2O Release Rate ($\mu g/hr\text{-}g\ UO_2$)
XBL 811-5087

Fig. 7

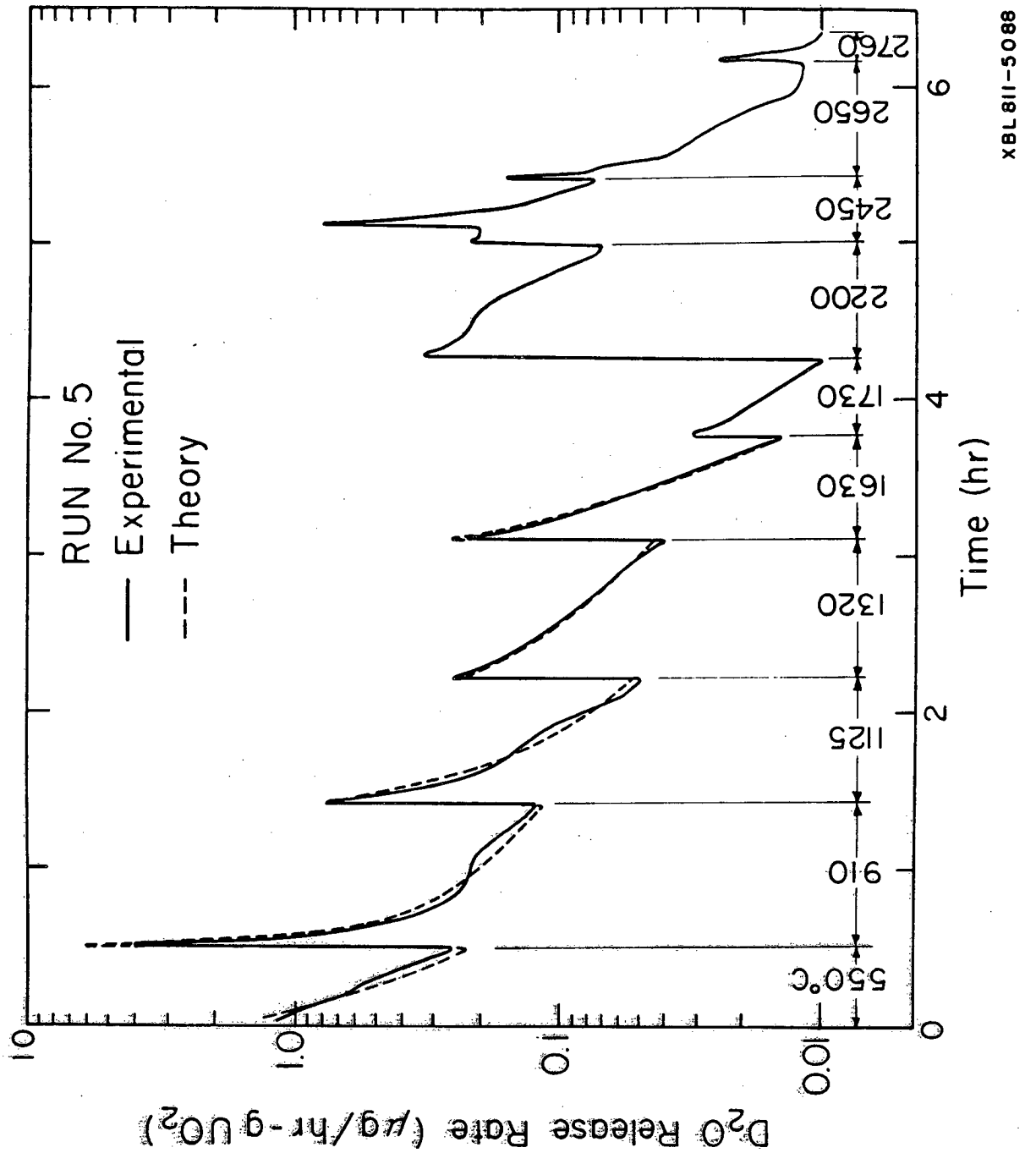
RUN No. 5
Experimental
Theory
550°C
910
1125
1320
1630
1730
2200
2450
2650
2760
Time (hr)
0
2
4
6
10
1.0
0.1
0.01
D2O Release Rate (μg/hr-g UO2)
XBL811-5088

Fig. 8

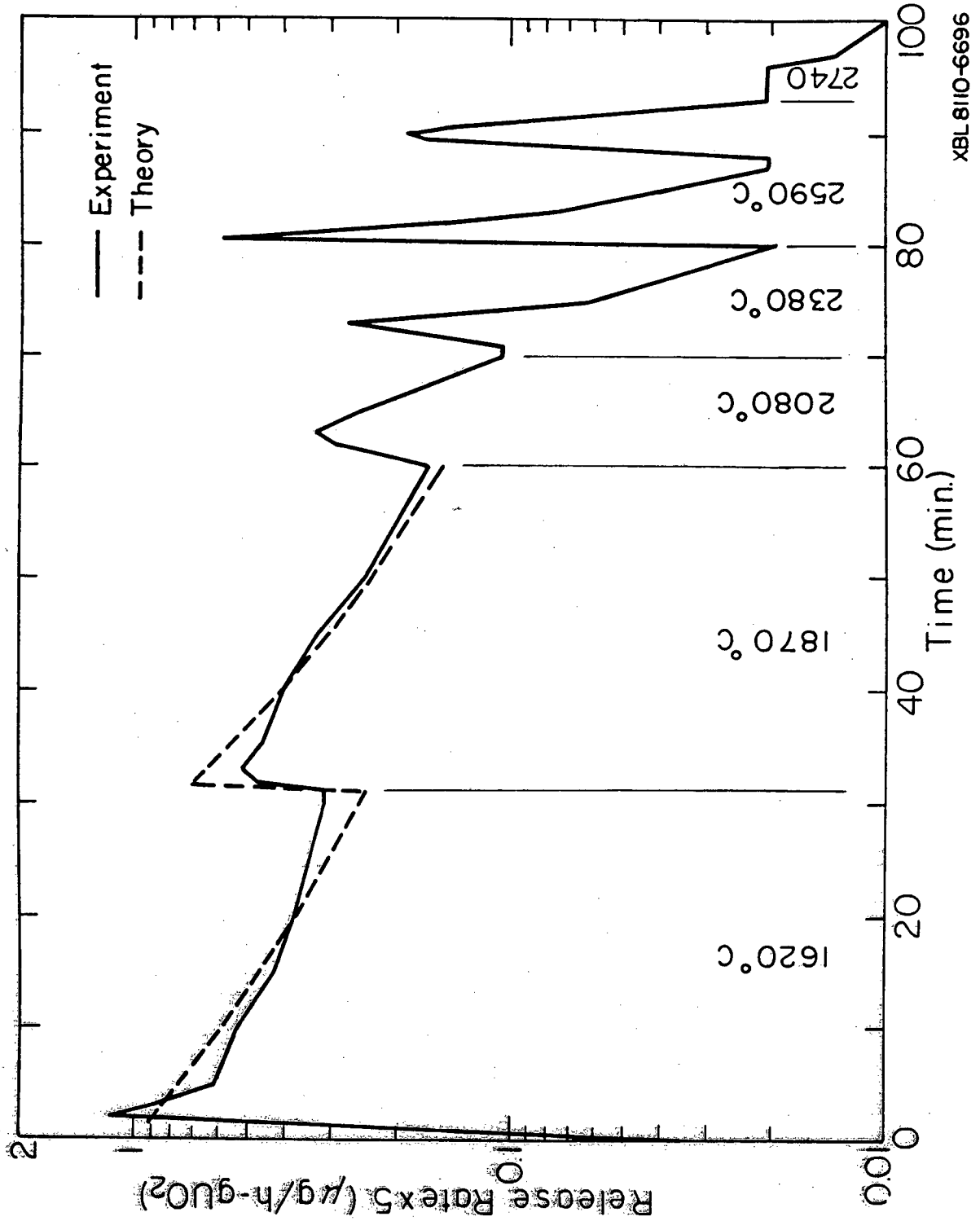
Release Rate x 5 (μg/h-gUO2)
Time (min.)
Experiment
Theory
1620°C
1870°C
2080°C
2380°C
2590°C
2740
XBL 8110-6696

Fig. 9

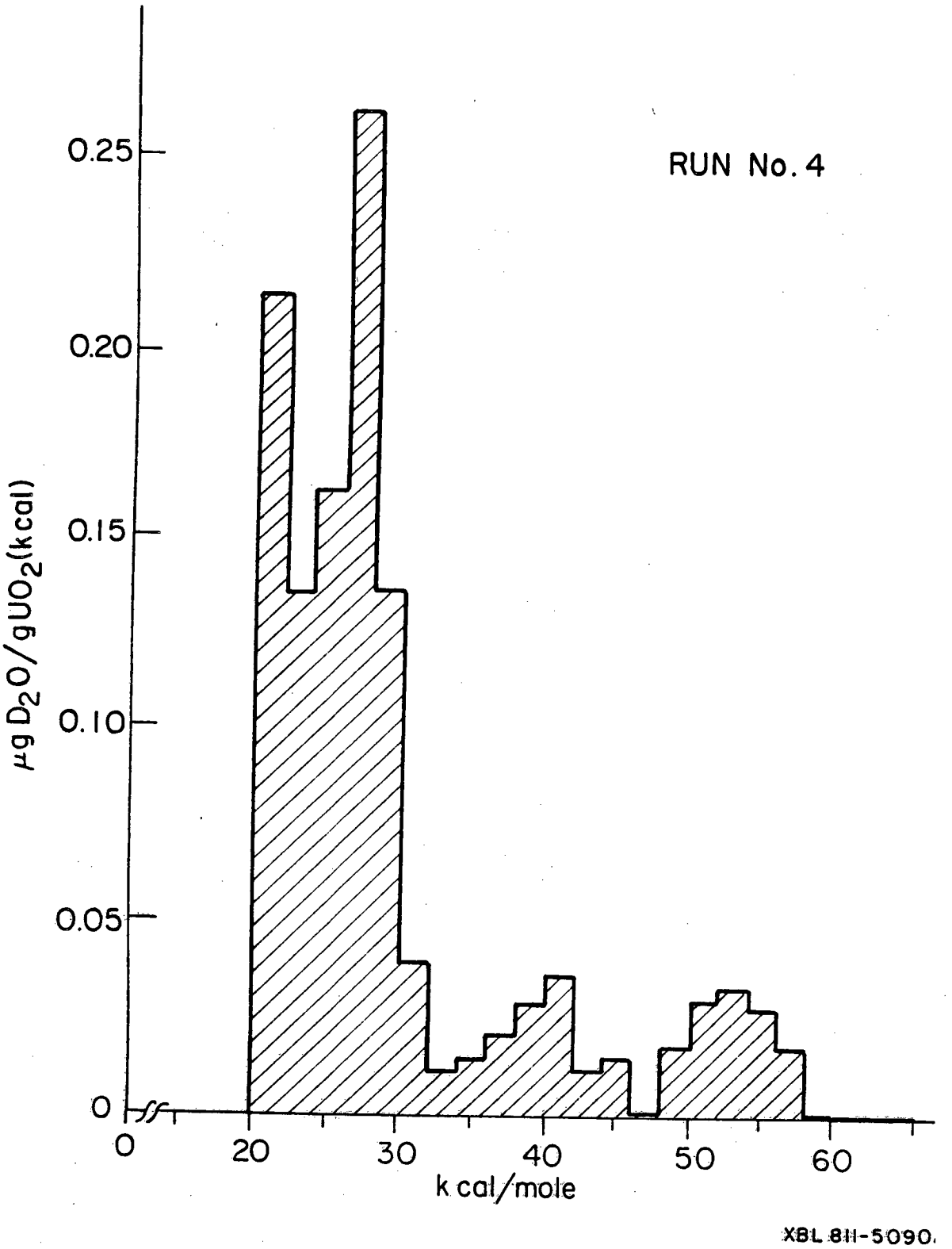
RUN No. 4
0.25
0.20
0.15
0.10
0.05
0
μg D2O/gUO2(kcal)
0
20
30
40
50
60
k cal/mole
XBL 811-5090

Fig. 10

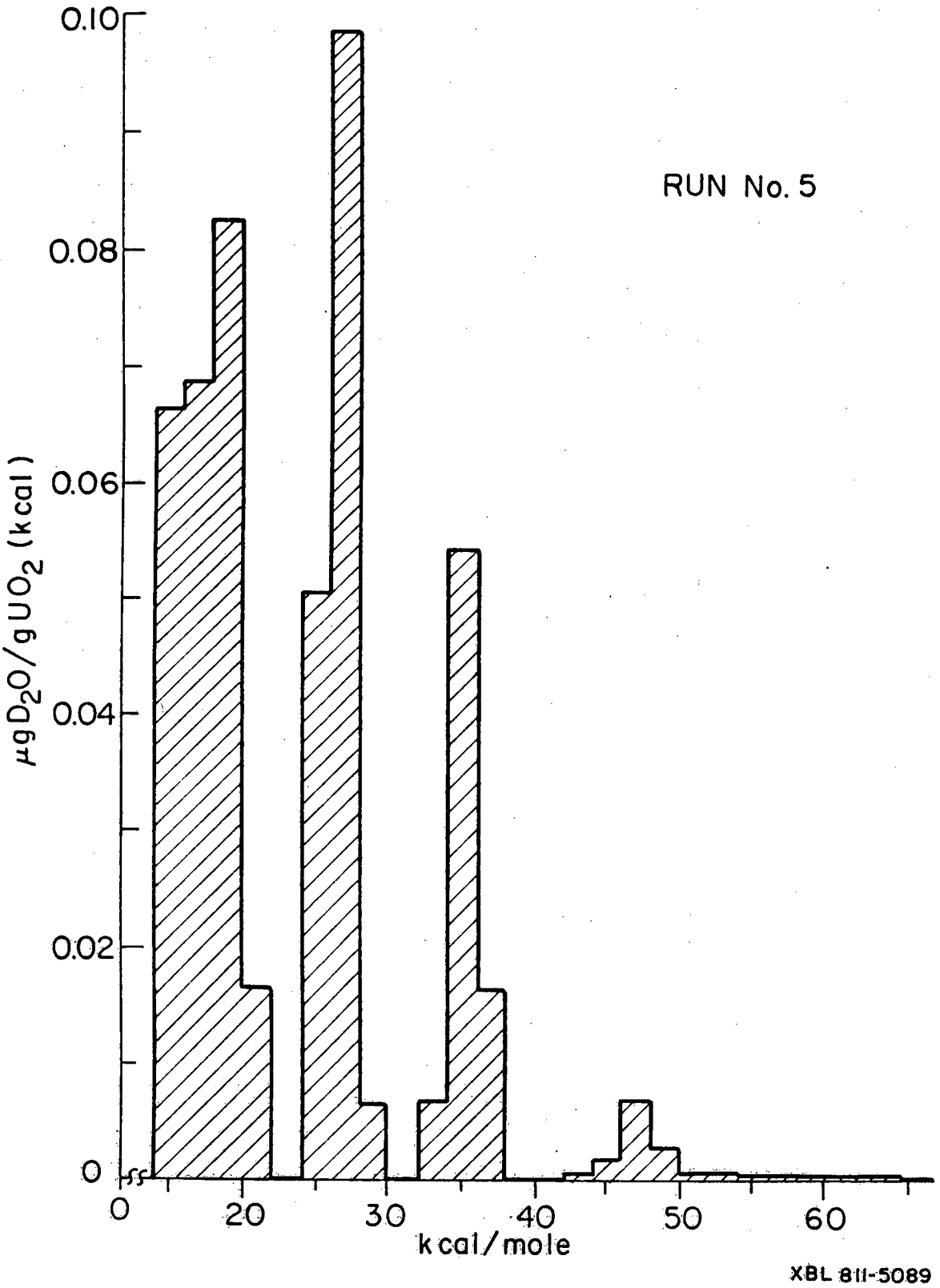
RUN No. 5
0.10
0.08
0.06
0.04
0.02
0
μgD2O/gUO2 (kcal)
0
20
30
40
50
60
kcal/mole
XBL 811-5089

Fig. 11

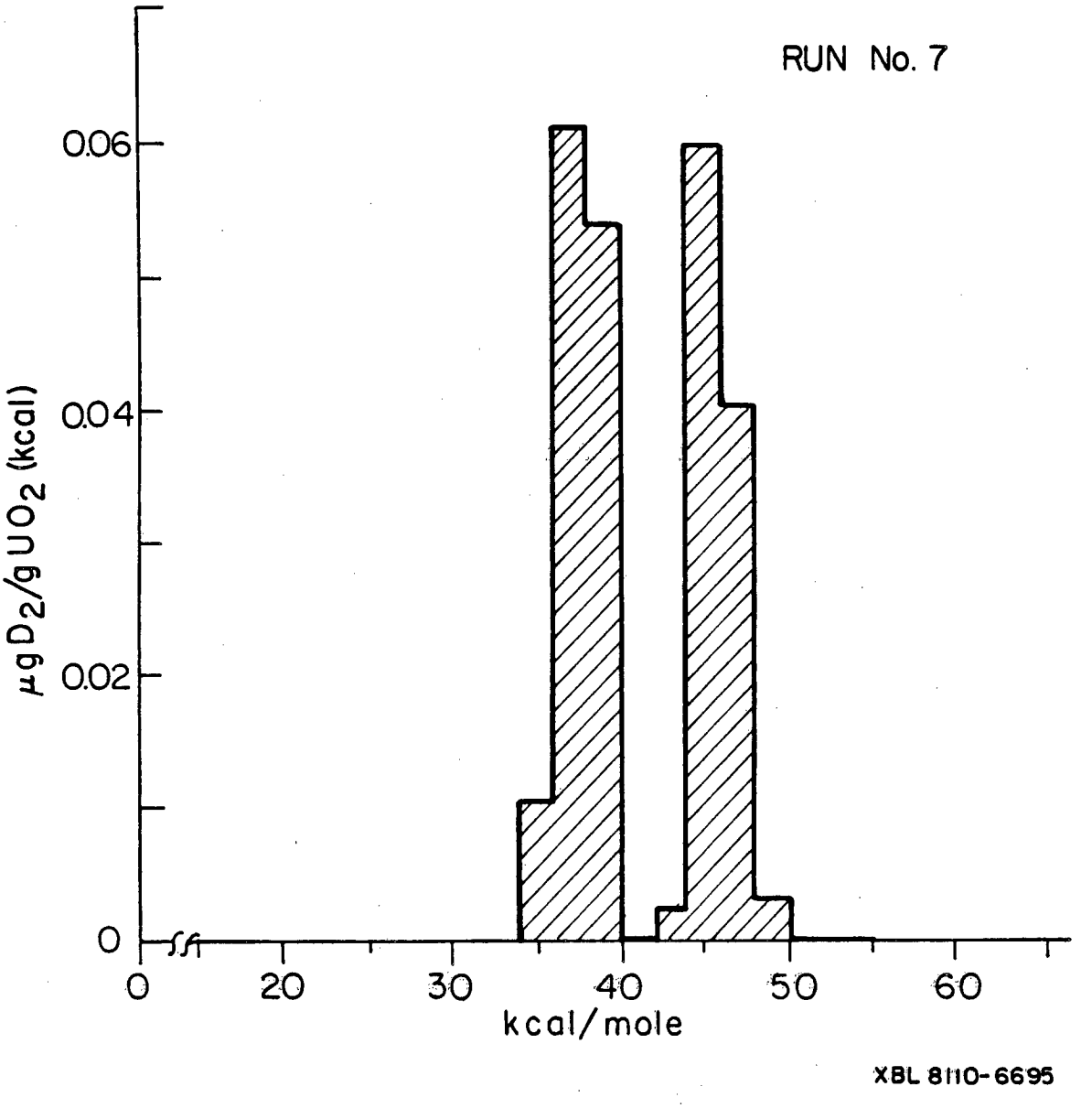
RUN No. 7
0.06
0.04
0.02
0
μg D2/g UO2 (kcal)
0
20
30
40
50
60
kcal/mole
XBL 8110-6695

Fig. 12

TECHNICAL INFORMATION DEPARTMENT
LAWRENCE BERKELEY LABORATORY
UNIVERSITY OF CALIFORNIA
BERKELEY, CALIFORNIA 94720